

Electronic-level calculations for semiconductor quantum dots: Deterministic numerical method using Green's functions

G. Cipriani

*Scuola Internazionale Superiore di Studi Avanzati, via Beirut 2-4, I-34014, Trieste, Italy
and INFN, Unità di Trieste, via Beirut 2-4, I-34014, Trieste, Italy*

M. Rosa-Clot

*Dipartimento di Fisica, Università di Firenze, L.go E. Fermi 2, I-50125, Firenze, Italy
and INFN, Sezione di Firenze, L.go E. Fermi 2, I-50125, Firenze, Italy*

S. Taddei

*Dipartimento di Fisica, Università di Firenze, L.go E. Fermi 2, I-50125, Firenze, Italy
and INFN, Unità di Firenze, L.go E. Fermi 2, I-50125, Firenze, Italy*

(Received 28 September 1999)

A numerical method to find the bound states of a low-dimensional quantum system is described. The method is used to calculate the energy levels and the wave functions of three-dimensional systems. In particular, the electronic level structure of self-assembled $\text{In}_x\text{Ga}_{1-x}\text{As}/\text{GaAs}$ quantum dots is studied.

INTRODUCTION

Recent growth techniques, as molecular-beam epitaxy (MBE) and atomic layer molecular-beam epitaxy (ALMBE), permit the fabrication of semiconductor microstructures that have aroused enormous interest both for their fundamental properties and potential applications in micro- and optoelectronics. Quantum wells (QW's), quantum wires, and quantum dots (QD's) allow one to attain one-, two-, and three-dimensional confinement of charge, respectively. The increasing amount of experimental data, coming from photoluminescence (PL) observations, needs a systematic theoretical analysis of the electronic levels of many different structures. A widely used approach to perform these calculations is the envelope function approximation with a multiband $\mathbf{k}\cdot\mathbf{p}$ Hamiltonian. In this case, the problem is to solve a set of eventually coupled Schrödinger equations. Therefore, it clearly arises the need of efficient numerical methods.

The available techniques for the computation of bound states of a quantum system fall into two main categories: the first one is based on the Hamiltonian operator, while the second category is based on the kernel of the Schrödinger equation for an infinitesimal time step (short-time propagator). The bound states can be obtained both by 'deterministic' and Monte Carlo methods. The latter have the important feature of facing problems with arbitrary dimensionality (see, for instance, Refs. 1 and 2), but a fundamental limit is the need of high statistics, and then large CPU time, to reduce the statistical errors. On the other hand, deterministic methods can be very accurate and relatively fast.

In this paper, we describe a deterministic technique that belongs to the second category and has good stability, good convergence properties, and a precision at least equivalent to that of efficient Hamiltonian methods (see, for instance, Ref. 3, for a comparison with a Fourier grid Hamiltonian method). In particular, it gives very high accuracy in delicate tunneling problems, where the localization properties of the

wave functions are important,⁴⁻⁶ as in the case of stacked QD's.⁷ A further feature of this technique is that, in some cases, we can factorize the short-time propagator as a tensorial product of one-dimensional free propagators and a diagonal tensor, with a huge gain in terms of computation and memory requirements. In the following, we refer to this method as "Green-function deterministic numerical diagonalization" (GFDND).

The main goal of this work is to show the application of the GFDND to the computation of the transition energies in QD structures. For the sake of simplicity, we use the one-band effective-mass approximation; therefore the Schrödinger equations for electron, heavy hole, and light hole are completely decoupled. Since here only ground-state energy calculations are performed, this approximation is justified.^{8,9}

The paper consists of four sections and two appendixes. In Sec. I we describe the numerical method. In Sec. II we define the potential model employed. In Sec. III we compare our numerical results with those obtained by photoluminescence analysis of $\text{In}_x\text{Ga}_{1-x}\text{As}/\text{GaAs}$ QD samples. The fourth section is the conclusion. In Appendixes A and B, we further discuss some details of the potential and the numerical method, respectively.

I. NUMERICAL METHOD

The short-time propagator, $K(\mathbf{x}, \mathbf{y}; \varepsilon)$, determines the evolution of the quantum system in a small time interval, ε , relating the wave function at the time $t_0 + \varepsilon$ to the wave function at the time t_0 ,

$$\psi(\mathbf{x}; t_0 + \varepsilon) = \int \cdots \int K(\mathbf{x}, \mathbf{y}; \varepsilon) \psi(\mathbf{y}; t_0) d^N y, \quad (1)$$

where N is the number of degrees of freedom. Since we are interested in the bound states only, we can use the Euclidean formulation. Then the oscillatory factors in the propagator

become Gaussians, and the numerical integrations are more stable and accurate. Therefore, ε is the imaginary time, and $K(\mathbf{x}, \mathbf{y}; \varepsilon)$ denotes the Euclidean propagator, which is given in Cartesian coordinates by

$$K(\mathbf{x}, \mathbf{y}; \varepsilon) = \frac{\sqrt{\det G_{pq}}}{(2\pi\varepsilon)^{N/2}} \exp\left\{-\frac{1}{2\varepsilon} G_{pq}(x^p - y^p)(x^q - y^q) - f(\mathbf{x}, \mathbf{y}; \varepsilon)\right\}, \quad (2)$$

where $\hbar=1$, G_{pq} is the ‘‘mass’’ tensor, and x^p , y^p are the components of \mathbf{x} , \mathbf{y} , respectively. The first term in the exponential corresponds to the kinetic part of the Hamiltonian, while the function $f(\mathbf{x}, \mathbf{y}; \varepsilon)$ represents the potential term. The explicit expression of the latter depends on the prescription chosen: the last point rule $f(\mathbf{x}, \mathbf{y}; \varepsilon) = \varepsilon V(\mathbf{x})$, for example, gives a short-time propagator correct up to $O(\varepsilon)$, while the symmetric expression $\varepsilon[V(\mathbf{x}) + V(\mathbf{y})]/2$ is correct up to $O(\varepsilon^2)$ (see, for instance, Ref. 2). A systematic expansion of the short-time propagator in powers of ε is also possible.^{5,6,10}

If E_α and $\psi_{(\alpha)}(\mathbf{x})$ are the eigenvalues and the eigenvectors of the Hamiltonian, respectively, then Eq. (1) becomes

$$\int \cdots \int K(\mathbf{x}, \mathbf{y}; \varepsilon) \psi_{(\alpha)}(\mathbf{y}) d^N y = e^{-\varepsilon E_\alpha} \psi_{(\alpha)}(\mathbf{x}), \quad (3)$$

which is an eigenvalue integral equation. Its solution yields directly the energy levels and the wave functions of the Hamiltonian. Equation (3) can be solved numerically as follows (finite interpolation method).³ Let us expand the unknown wave function $\psi_{(\alpha)}(\mathbf{x})$ on some basis of interpolating functions. In the multidimensional case, it is convenient to choose a basis given by the tensorial product of one-dimensional functions. Thus, in general,

$$\psi_{(\alpha)}(\mathbf{x}) \approx \sum_{i_1=1}^{M_1} \cdots \sum_{i_N=1}^{M_N} a_{(\alpha)}^{i_1, \dots, i_N} \varphi_{i_1}(x^1), \dots, \varphi_{i_N}(x^N). \quad (4)$$

In particular, as one-dimensional interpolating functions, we use piecewise polynomials of order n even. More precisely, since high-order Lagrange polynomials may lead to unwanted oscillations, we take only the piece between the two central interpolation points. Then we repeat the process over all inner points, while the initial and final points are interpolated by the left and right side of the Lagrange polynomials, respectively. Let us denote such polynomials with the symbols $l_i(x)$. Thus expression (4) becomes

$$\psi_{(\alpha)}(\mathbf{x}) \approx \sum_{i_1=1}^{M_1} \cdots \sum_{i_N=1}^{M_N} \psi_{(\alpha)}^{i_1, \dots, i_N} l_{i_1}(x^1), \dots, l_{i_N}(x^N), \quad (5)$$

where now the coefficients $\psi_{(\alpha)}^{i_1, \dots, i_N}$ are just the values of the function $\psi_{(\alpha)}(\mathbf{x})$ in the interpolating points $(x_{i_1}^1, \dots, x_{i_N}^N)$. If we substitute this expression in Eq. (3), we obtain

$$\sum_{i_1=1}^{M_1} \cdots \sum_{i_N=1}^{M_N} \tilde{K}_{i_1, \dots, i_N}(\mathbf{x}; \varepsilon) \psi_{(\alpha)}^{i_1, \dots, i_N} \approx e^{-\varepsilon E_\alpha} \psi_{(\alpha)}(\mathbf{x}), \quad (6)$$

where

$$\tilde{K}_{i_1, \dots, i_N}(\mathbf{x}; \varepsilon) = \int \cdots \int K(\mathbf{x}, \mathbf{y}; \varepsilon) l_{i_1}(y^1), \dots, l_{i_N}(y^N) \times d^N y. \quad (7)$$

Since the functions $l_i(x)$ are given, integral (7) can be explicitly calculated by analytical or numerical techniques. We can now find the coefficients $\psi_{(\alpha)}^{i_1, \dots, i_N}$ by selecting $M^1 \times \cdots \times M^N$ distinct grid points $(x_{i_1}^1, \dots, x_{i_N}^N)$ and solving the following eigenvalue problem (collocation method),

$$\sum_{j_1=1}^{M_1} \cdots \sum_{j_N=1}^{M_N} \tilde{K}_{i_1, \dots, i_N, j_1, \dots, j_N}^\varepsilon \psi_{(\alpha)}^{j_1, \dots, j_N} \approx e^{-\varepsilon E_\alpha} \psi_{(\alpha)}^{i_1, \dots, i_N}, \quad (8)$$

where

$$\tilde{K}_{i_1, \dots, i_N, j_1, \dots, j_N}^\varepsilon \equiv \tilde{K}_{j_1, \dots, j_N}^\varepsilon[(x_{i_1}^1, \dots, x_{i_N}^N); \varepsilon]. \quad (9)$$

The multidimensional tensor $\tilde{K}_{i_1, \dots, i_N, j_1, \dots, j_N}^\varepsilon$ becomes very large as the degrees of freedom of the system increase; in practice, already the case of three degrees of freedom is quite difficult to handle. However, for a wide range of physical systems, the mass tensor G_{pq} is constant and diagonal. Moreover, since the time step ε can be chosen very small,³ we can take $f(\mathbf{x}, \mathbf{y}; \varepsilon) = \varepsilon V(\mathbf{x})$, and the potential term can be put out of the integrals. In this case, the numerical problem is much simpler because expression (9) simplifies as

$$\begin{aligned} \tilde{K}_{i_1, \dots, i_N, j_1, \dots, j_N}^\varepsilon \\ \equiv \tilde{K}_{i_1, j_1}^{1, \varepsilon} \cdots \tilde{K}_{i_N, j_N}^{N, \varepsilon} \exp\{-\varepsilon V[(x_{i_1}^1, \dots, x_{i_N}^N)]\}, \end{aligned} \quad (10)$$

where

$$\tilde{K}_{i_p, j_p}^{p, \varepsilon} = \int \sqrt{\frac{m_p}{2\pi\varepsilon}} \exp\left\{-\frac{m_p}{2\varepsilon}(x_{i_p}^p - y)^2\right\} l_{j_p}(y) dy \quad (11)$$

and

$$m_p = G_{pp}. \quad (12)$$

Therefore, we can factorize the propagator as a tensorial product of one-dimensional free propagator matrices multiplied by the diagonal tensor corresponding to the potential term. This means that, if we solve the eigenvalue problem by iterative techniques, we need much less effort both in terms of computation and memory requirements, and it becomes possible to deal also with three or four-dimensional problems.

As a final remark, we note that in Eq. (8) there are not restrictions on the choice of the distribution of grid points. Therefore, we can choose an appropriate distribution, according to the shapes of the wave functions, in order to obtain a better accuracy with the same number of points. This

is equivalent to saying that we can choose an appropriate transformation of variables that maps the original interval of integration onto a new one and then discretize the new variables. In particular, we can map an infinite interval onto a finite one. Thus we have the further advantage to take correctly into account the boundary conditions by simply requiring that the wave functions vanish on the border of the interval.

Cylindrical coordinates

The previous discussion is limited to the Cartesian coordinates. We now consider the case of a three-dimensional potential with a cylindrical symmetry. Then we can separate one angular variable, and the propagator can be written in the following way (see, for example, Ref. 11)

$$K(\mathbf{r}, \mathbf{r}'; \varepsilon) = \sum_{m=-\infty}^{+\infty} \frac{1}{\sqrt{\rho\rho'}} g_m(\rho, z, \rho', z'; \varepsilon) \frac{1}{2\pi} e^{im(\theta-\theta')}, \quad (13)$$

where $\mathbf{r} \equiv (\rho, \theta, z)$ are the cylindrical coordinates. Since the quantum system has a cylindrical symmetry, the azimuthal quantum number m is conserved. Thus the contributions of different values of m can be separated. If we define the cylindrical wave functions $\phi_{(am)}(\rho, z)$ by

$$\psi_{(am)}(\mathbf{r}) = \frac{\phi_{(am)}(\rho, z)}{\sqrt{\rho}} \frac{e^{im\theta}}{2\pi}, \quad (14)$$

where $\psi_{(am)}(\mathbf{r})$ are the complete eigenfunctions of the Hamiltonian, they satisfy the integral equation

$$\int g_m(\rho, z, \rho', z'; \varepsilon) \phi_{(am)}(\rho', z') d\rho' dz' = e^{-\varepsilon E_{(am)}} \phi_{(am)}(\rho, z). \quad (15)$$

The short-time cylindrical propagator $g_m(\rho, z, \rho', z'; \varepsilon)$ is given by

$$g_m(\rho, z, \rho', z'; \varepsilon) = k_m^\rho(\rho, \rho'; \varepsilon) k_m^z(z, z'; \varepsilon) e^{-f(\rho, z, \rho', z'; \varepsilon)}. \quad (16)$$

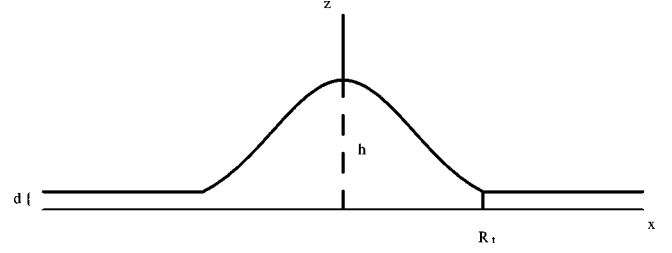


FIG. 1. Schematic cross section of the InAs cluster in the (100) plane through the top of the dot.

As usual, $f(\rho, z, \rho', z'; \varepsilon)$ depends on the prescription chosen for the potential, while

$$k_m^\rho(\rho, \rho'; \varepsilon) = \sqrt{\frac{m_\rho}{2\pi\varepsilon}} \sqrt{2\pi m_\rho} \frac{\rho\rho'}{\varepsilon} e^{-m_\rho\rho\rho'/\varepsilon} I_m\left(m_\rho \frac{\rho\rho'}{\varepsilon}\right) \times e^{-m_\rho(\rho-\rho')^2/2\varepsilon}, \quad (17)$$

$$k_m^z(z, z'; \varepsilon) = \sqrt{\frac{m_z}{2\pi\varepsilon}} e^{-m_z(z-z')^2/2\varepsilon}, \quad (18)$$

and $I_m(x)$ are the modified Bessel functions. Again, if we choose the last point prescription for the potential term, and we substitute expression (16) in Eq. (15), the resulting eigenvalue equation can be written as a tensorial product of one-dimensional matrices multiplied by a diagonal tensor, as in the Cartesian case. Then we can find the eigenvalues and the eigenfunctions of the Hamiltonian in the usual way.

II. $\text{In}_x\text{Ga}_{1-x}\text{As}/\text{GaAs}$ QUANTUM DOTS

The simplest model for describing a single $\text{In}_x\text{Ga}_{1-x}\text{As}/\text{GaAs}$ QD is an envelope function approximation using a one-band Hamiltonian with constant effective masses and a three-dimensional potential, which has the same geometrical shape of the QD and includes a constant¹² or numerically computed¹³ strain contribution. More recent models are based on multiband $\mathbf{k}\cdot\mathbf{p}$ Hamiltonians and realistic strain distributions.^{8,9,14,15} Furthermore, an alternative approach is based on pseudopotential calculations.¹⁶⁻¹⁸ Fi-

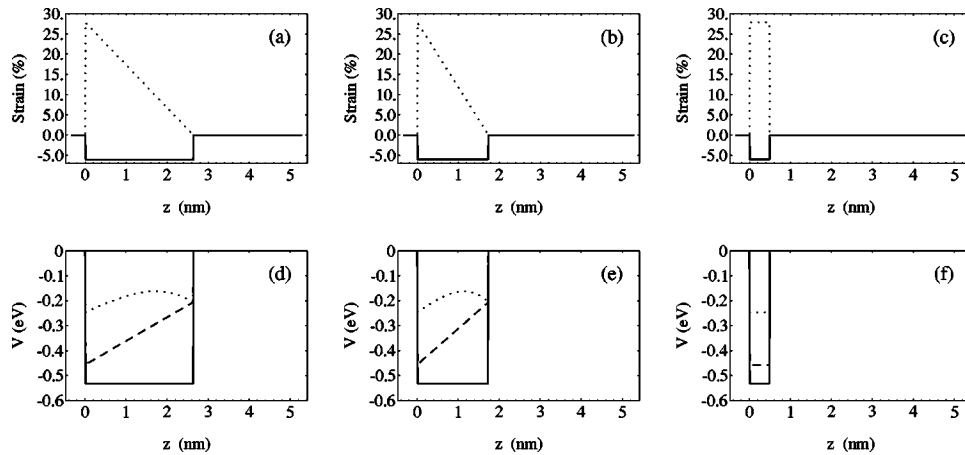


FIG. 2. Hydrostatic (solid line) and biaxial (dotted line) components of the strain, and electron (solid line), heavy-hole (dashed line), and light-hole (dotted line) confinement potential ($h=8$ ML, $d=1.5$ ML, $\Lambda=0$ ML) for line scans in the $[001]$ direction: (a),(d) along a line through the top of the dot; (b),(e) and (c),(f) along lines at distances $R/2$ and R_1 from the center of the dot, respectively.

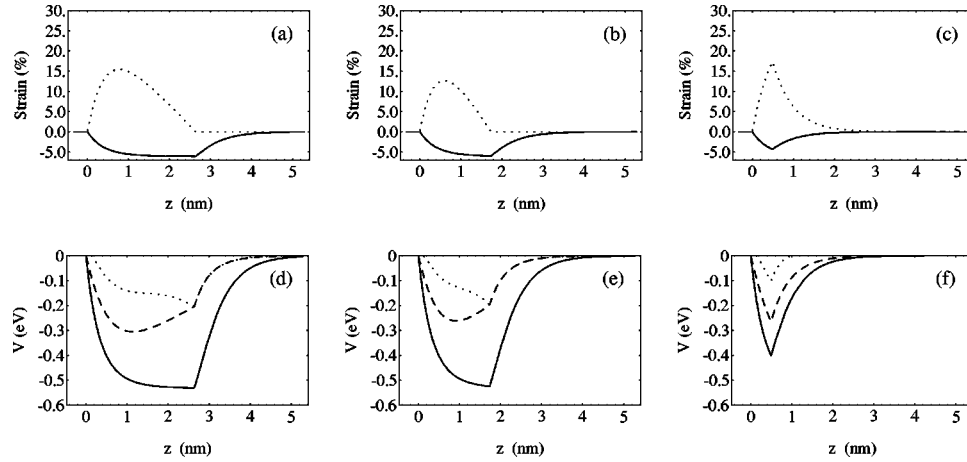


FIG. 3. Hydrostatic (solid line) and biaxial (dotted line) components of the strain, and electron (solid line), heavy-hole (dashed line), and light-hole (dotted line) confinement potential ($h=8$ ML, $d=1.5$ ML, $\Lambda=1.5$ ML) for line scans in the [001] direction: (a),(d) along a line through the top of the dot; (b),(e) and (c),(f) along lines at distances $R/2$ and R_t from the center of the dot, respectively.

nally, the indium segregation effects, and the Coulomb interaction must be considered.

Here we adopt the following approach. We use a one-band Hamiltonian with constant effective masses. Moreover, an analytical approximation of a realistic strain distribution is used, and also the indium segregation is taken into account. Finally, the Coulomb interaction is computed perturbatively.¹⁹ The one-band approximation gives significant differences in the calculation of the excited states, but only small corrections for the ground states.^{8,9} Since here we are interested only in the latter, this simplified approach is justified.

The potential is defined as follows. We suppose that the QD has a cylindrical symmetry and a Gaussian height profile with standard deviation σ and maximum height h (in fact, the shape and the dimension of the QD's depend on the growth conditions, and, for example, QDs with either cylindrical^{20–22} or pyramidal^{13,14,23} symmetries can be obtained). Moreover, we must take into account that the QD resides on a continuous wetting layer with thickness d . Thus, if we define the aspect ratio, $Q=h/4\sigma$, the height profile of the QD is

$$S(\rho) = \begin{cases} h e^{-8Q^2\rho^2/h^2} & \text{if } \rho < R_t \\ d & \text{if } \rho \geq R_t. \end{cases} \quad (19)$$

The parameter R_t is the distance between the dot's axis and the point where the QD merges in the wetting layer, and it is given by

$$R_t = \frac{h}{4Q} \sqrt{2 \ln \frac{h}{d}} \quad (20)$$

(a schematic drawing of the dot is shown in Fig. 1). Then we write the confinement potential as

$$V^e(\rho, z) = E_c\{x[z, S(\rho)], z, S(\rho)\} - E_c[0, z, S(\rho)], \quad (21)$$

$$V^{hh}(\rho, z) = E_v^{hh}\{0, z, S(\rho)\} - E_v^{hh}\{x[z, S(\rho)], z, S(\rho)\}, \quad (22)$$

$$V^{lh}(\rho, z) = E_v^{lh}\{0, z, S(\rho)\} - E_v^{lh}\{x[z, S(\rho)], z, S(\rho)\}. \quad (23)$$

where $x[z, S(\rho)]$ is the indium composition, depending both on the nominal composition x_0 and the indium segregation length²⁴ Λ , while the functions E_c , E_v^{hh} , and E_v^{lh} are the

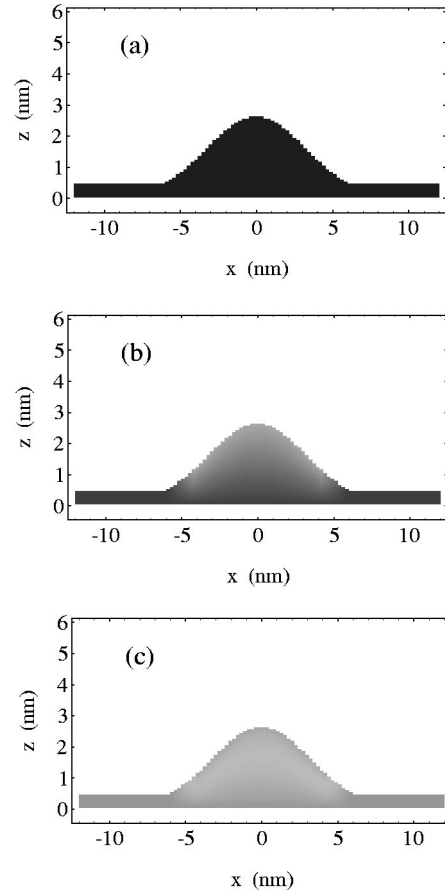


FIG. 4. Confinement potential ($h=8$ ML, $d=1.5$ ML, $\Lambda=0$ ML) for electrons (a), heavy holes (b), and light holes (c) in the (100) plane through the top of the dot. The gray scale is the same for all plots.

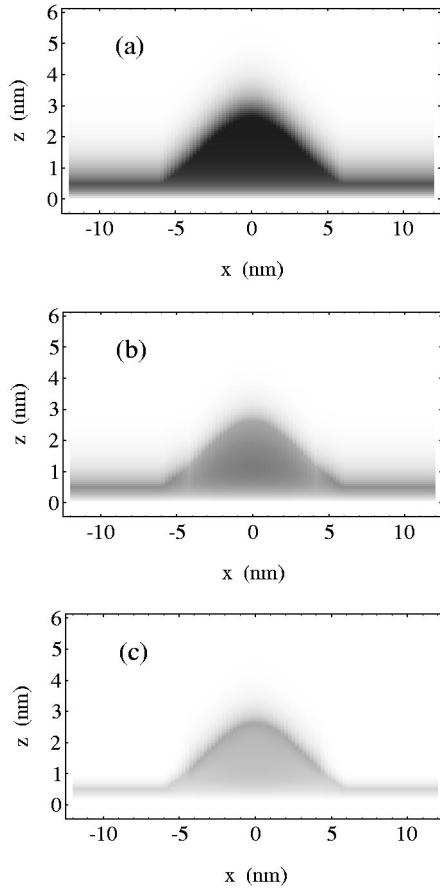


FIG. 5. Confinement potential ($h=8$ ML, $d=1.5$ ML, $\Lambda=1.5$ ML) for electrons (a), heavy holes (b), and light holes (c) in the (100) plane through the top of the dot. The gray scale is the same for all plots.

edges of the energy bands of the $\text{In}_x\text{Ga}_{1-x}\text{As}$. All previous functions are defined in Appendix A. In Figs. 2, and 3 we plot the confinement potentials along line scans in the [001] direction. In Figs. 4, and 5 we show their density plots.

After the potential has been defined, the transition energies are computed as $\Delta E_\alpha = E_\alpha^e + E_\alpha^{hh(lh)} + E_g^{\text{GaAs}} + E_C$, where E_α^e and $E_\alpha^{hh(lh)}$ are the single-particle confinement energies, E_g^{GaAs} is the energy gap between the valence and conduction bands of the GaAs, and E_C is the Coulomb energy.

III. RESULTS

In this section we study one particular structure of $\text{In}_x\text{Ga}_{1-x}\text{As}/\text{GaAs}$ QD's. A layer of InAs was grown by MBE in the Stranski-Krastanow mode on a (001) GaAs wafer, close to the two-dimensional to three-dimensional transition.^{25,26} The substrate was not rotated during the growth in order to have a continuous variation of InAs coverage across the wafer from below to above the critical coverage for the 2D–3D transition. After the deposition at 580 °C of a GaAs buffer layer and a 210 s growth interruption, the dots were formed at 500 °C. Finally, the structure was capped by a 20-nm-thick GaAs layer grown at 500 °C that acts as an upper confining layer.

The InAs coverage of the samples varies between about 1.3 ML and 2.0 ML (see Refs. 21 and 22). The analysis of

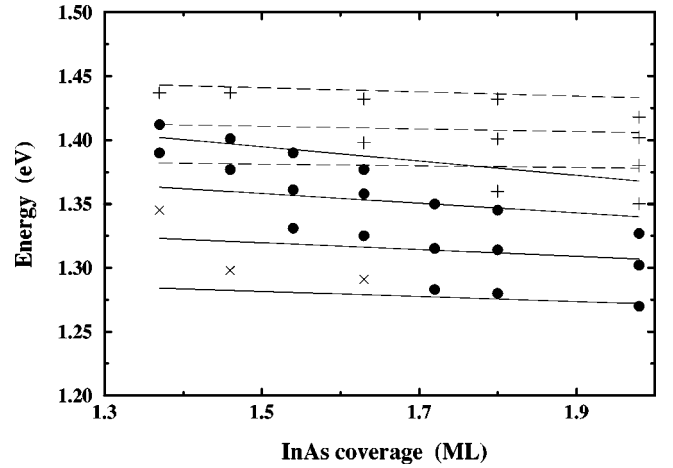


FIG. 6. Experimental peak energies from the PL spectra at 10 K after deconvolution into Gaussian components and theoretical predictions for the transition energies for the different QD families, as a function of the InAs coverage. The solid circles refer to emissions from the QD's for excitation above the GaAs band gap. The crosses refer to PL bands observed after excitation below the GaAs band gap. The pluses refer to additional emissions from the QD's for high excitation conditions. The solid lines are the theoretical transition energies between the electron and the heavy-hole ground states. The dashed lines are the theoretical transition energies between the electron and the light-hole ground states.

uncapped samples, grown under the same conditions, by atomic force microscope (AFM) has shown that the QD heights h lie within the range 2–4 nm,²⁷ while the aspect ratios Q have a large experimental uncertainty but seem to increase with increasing h . Moreover, an x-ray analysis of QW samples (with $d \sim 1$ ML), grown under similar conditions,^{28,29} gives a value for the segregation length Λ between 1.5 and 2 ML. This value also allows one to fit the QW photoluminescence data by an envelope function approach (although the envelope function approximation for ultrathin InAs layers could not be completely justified,³⁰ it has been shown that such an approximation can give quite accurate results³¹).

A photoluminescence analysis of these QD samples has already been reported in Refs. 21 and 22. The peak energies of the deconvoluted bands of the PL spectra at 10 K of seven QD samples, under cw excitation at 632.8 nm, at an excitation power density of 50 W/cm², are plotted in Fig. 6 as a function of the InAs coverage (solid circles). Moreover, the peak positions of additional, less intense, PL bands clearly observed only under cw excitation below the GaAs band-gap energy (crosses), or for high excitation conditions (pluses) are also reported. The experimental data show discrete emission bands for any given InAs coverage. Moreover, the PL bands shift slightly to lower energies for increasing InAs coverage. The observed pattern of discrete emission energies has been explained by assuming that, under the previously described growth conditions, the QD's nucleate in distinct families characterized by well-defined QD sizes. Correspondingly, for a given InAs coverage, the discrete emission bands can be attributed to radiative recombination from the ground states of QD's belonging to different families. This interpretation is supported by PL time-resolved measurements, as reported in Refs. 21 and 22. The time-resolved

TABLE I. Material properties of GaAs and InAs used in the calculations. Symbols are explained in the text.

	a_0 (nm)	C_{11} (N/m ²)	C_{12} (N/m ²)	ϵ_r
GaAs	0.565325	11.88	5.38	12.5
InAs	0.60583	8.33	4.526	15.2
	$E_{v,av}^0$ (eV)	a_c (eV)	a_v (eV)	b (eV)
GaAs	-6.92	-7.17	1.16	-1.7
InAs	-6.67	-5.08	1.00	-1.8

measurements show that for each sample with a given InAs coverage the emissions at higher energies do not result from excited states, that, indeed, can be observed only after high excitation.

We show now that a numerical analysis of the electronic level structure strongly supports the hypothesis that the observed quantization pattern in the sizes of the self-assembled QD's, and therefore in the emission spectra, can be basically ascribed to the quantization of the QD heights at steps of 1 ML.^{21,22}

Accordingly with the previous considerations about the QD structures, we assume that (i) the thickness of the InAs wetting layer (WL), which must be lower than the InAs coverage, increases linearly with the coverage from $d=1.2$ ML to $d=1.8$ ML. (ii) The QD's have heights between 7 – 10 ML quantized with steps of 1 ML. (iii) The aspect ratio Q lies in the range 0.3–0.4, increases with h , and is quantized with steps $\Delta Q=0.027$. (iv) The segregation length Λ is equal to 1.5 ML. In the following we describe the results obtained, while in Appendix B we discuss the stability and the accuracy of the GFDND. The complete list of parameters is given in Tables I and II.

In Fig. 7, we plot the transition energies without the Coulomb corrections versus the QD height, for a fixed InAs wetting-layer thickness $d=1.2$. This plot shows that there are no excited-state transitions in QD's of these dimensions, while there are both electron-heavy-hole and electron-light-hole ground-state transitions. Then, by taking into account the exciton binding energy and plotting the corrected transition energies versus the InAs coverage, we obtain the graph in Fig. 6. This shows a surprisingly good agreement between the observed transition pattern and the predicted one. The small difference in the slopes of the experimental and theoretical lines occurs also for QW samples grown under similar conditions and can depend on the limits of the envelope function approach for such ultra-thin QW's. Finally we observe that, as shown by multiband calculations,^{8,9} excited states cannot be completely excluded, especially in the larg-

TABLE II. Effective masses used in the calculations.

	$m_c(m_0)$	$m_r(m_0)$
Electron	0.067	0.067
Heavy hole	0.45	0.11
Light hole	0.09	0.21

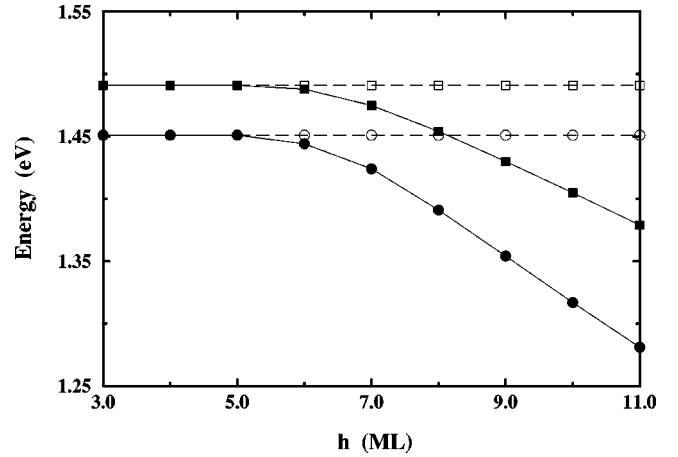


FIG. 7. Theoretical transition energies vs QD height, without Coulomb corrections, for fixed InAs wetting-layer thickness ($d=1.2$).

est QD's. However, the presence of a few further transitions should not change the main features of the pattern obtained.

CONCLUSIONS

In this paper we have described a numerical method (GFDND), based on the diagonalization of the short-time propagator, to solve the Schrödinger equation. We have discussed the general multidimensional case and shown that, in some cases, we can factorize the short-time propagator as a tensorial product of one-dimensional free propagators and a diagonal tensor. This gives a huge gain in terms of memory requirements and allows one to attain quite easily problems with 3–4 degrees of freedom.

We have used the GFDND to solve a system of decoupled three-dimensional Schrödinger equations, which describes a $\text{In}_x\text{Ga}_{1-x}\text{As}/\text{GaAs}$ QD with cylindrical symmetry and lying on a thin wetting layer, in a one-band effective-mass approximation. The potential used takes into account both the strain distribution in and around the QD and the indium segregation, while the exciton binding energy has been calculated in first-order perturbation theory and typically amounts to 10–30 meV.

We have studied a particular structure of InAs/GaAs QD's, and we have found a quantization pattern that can be basically ascribed to the transition between electron-hole ground states in QD's with quantized heights differing by 1 ML.

ACKNOWLEDGMENTS

We would like to thank L. C. Andreani, M. Berti, F. Bogani, P. Borri, A. Bosacchi, M. Colocci, S. Franchi, S. Sanguinetti, and A. Zunger for many helpful discussions and important suggestions. Work at LENS is supported by the European Community under the TMR Program, Contract No. ERBFMGECT950017. This work has also been supported by CNR-Progetto Finalizzato MADESS II.

APPENDIX A: POTENTIAL MODEL

If we assume that the indium composition is constant inside and zero outside the QD and we neglect the strain ef-

fects, the confining potential for the electrons (holes) is a steplike function given by the difference in the absolute energy of the conduction- (valence-) band edges in $\text{In}_x\text{Ga}_{1-x}\text{As}$ and GaAs. Actually, the strain modifies the $\text{In}_x\text{Ga}_{1-x}\text{As}$ band gap.

For a strained QW, such modifications can be obtained in the following way (see, for example, Refs. 32 and 33). An absolute energy scale for the semiconductor band offset is defined by giving the value of the unstrained average valence band $E_{v,\text{av}}^0(x)$, where x is the indium composition. The offset of the unstrained conduction band is $E_c^0(x) = E_{v,\text{av}}^0(x) + [\Delta_0(x)]/3 + E_g(x)$, where $\Delta_0(x)$ is the spin-orbit splitting, and $E_g(x)$ is the unstrained energy gap. These quantities depend on the indium composition: (a) the average valence-band position is derived by linear interpolation between the values for the pure materials, (b) $\Delta_0(x) = 0.341 - 0.09x + 0.14x^2$, and (c) $E_g(x) = 1.519 - 1.584x + 0.475x^2$ (we neglect small variations depending on the temperature); in the following, the indium composition dependence will be understood. The strain-induced shift of the conduction band δE_c depends only on the hydrostatic component of the strain

$$\delta E_c = a_c(\epsilon_{xx} + \epsilon_{yy} + \epsilon_{zz}), \quad (\text{A1})$$

where ϵ_{xx} , ϵ_{yy} , and ϵ_{zz} are the components of the strain tensor given by

$$\epsilon_{xx} = \epsilon_{yy} = \frac{a_{\text{GaAs}} - a_{\text{In}_x\text{Ga}_{1-x}\text{As}}}{a_{\text{In}_x\text{Ga}_{1-x}\text{As}}}, \quad (\text{A2})$$

$$\epsilon_{zz} = -2 \frac{C_{12}}{C_{11}} \epsilon_{xx}, \quad (\text{A3})$$

a_{GaAs} and $a_{\text{In}_x\text{Ga}_{1-x}\text{As}}$ are the lattice constants, and C_{11} and C_{12} are the elastic constants. Hence,

$$E_c = E_c^0 + \delta E_c. \quad (\text{A4})$$

Moreover, if we assume that the heavy-hole and the light-hole bands can be completely decoupled, we have

$$E_v^{hh} = E_{v,\text{av}}^0 + \frac{\Delta_0}{3} + \delta E_{v,h} - \frac{1}{2} \delta E_{v,b}, \quad (\text{A5})$$

$$E_v^{lh} = E_{v,\text{av}}^0 - \frac{\Delta_0}{6} + \delta E_{v,h} + \frac{1}{4} \delta E_{v,b} + \frac{1}{2} \sqrt{\Delta_0^2 + \Delta_0 \delta E_{v,b} + \frac{9}{4} (\delta E_{v,b})^2}, \quad (\text{A6})$$

where

$$\delta E_{v,h} = a_v(\epsilon_{xx} + \epsilon_{yy} + \epsilon_{zz}), \quad (\text{A7})$$

and $\delta E_{v,b}$ is related to the biaxial component of the strain $\epsilon_b = 2\epsilon_{zz} - \epsilon_{xx} + \epsilon_{yy}$ by

$$\delta E_{v,b} = b \epsilon_b. \quad (\text{A8})$$

All lattice parameters, and the deformation potentials a_c , a_v , and b , depend on the indium composition. They are obtained by linear interpolation between the pure material parameters, given in Table I.

In the case of a strained QD, a rigorous approach would require a numerical computation of the strain tensor in each unit cell of the structure (see, Refs. 13 and 14); however, we adopt here a partially simplified approach. As a first approximation, we could assume that the dependence of the strain tensor on the lattice parameters is the same of a QW. In such a case, the strain-induced correction, which is function of the indium composition, is constant inside and zero outside the QD. In fact, on the basis of the strain distributions reported in Refs. 13, and 14, we note that (a) the hydrostatic component of the strain is almost constant inside and zero outside the QD, and its value is almost the same of a strained QW and (b) the biaxial component of the strain is larger at the bottom of the QD and decreases almost linearly towards the top. Therefore, according to these considerations, we assume that (a) the energy shift induced by the hydrostatic component of the strain is given by the Eqs. (A1), (A7), and (A3); and (b) the energy shift induced by the biaxial component of the strain is given by Eq. (A8) with

$$\epsilon_b \equiv \epsilon_b[z, S(\rho)] = \begin{cases} 0 & \text{if } z < 0 \\ \frac{\epsilon_b^1[S(\rho)] - \epsilon_b^0}{S(\rho)} z + \epsilon_b^0 & \text{if } 0 \leq z \leq S(\rho) \\ \epsilon_b^1[S(\rho)] & \text{if } z > S(\rho), \end{cases} \quad (\text{A9})$$

and

$$\epsilon_b^1[S(\rho)] = \begin{cases} \frac{\epsilon_b^0}{2 \text{ ML}} [d + 2 \text{ ML} - S(\rho)] & \text{if } d \leq S(\rho) < d + 2 \text{ ML} \\ 0 & \text{if } S(\rho) \geq d + 2 \text{ ML}. \end{cases} \quad (\text{A10})$$

The parameter ϵ_b^0 is the biaxial strain inside a QW, and $S(\rho)$ is the QD height profile defined in Eq. (19). When $S(\rho) \geq d + 2 \text{ ML}$, the function $\epsilon_b[z, S(\rho)]$ decreases linearly from the bottom ($\epsilon_b = \epsilon_b^0$) to the top ($\epsilon_b = 0$) of the QD. In the limit $S(\rho) \rightarrow d$, it becomes constant and equal to ϵ_b^0 (we remind that the dependence on the indium composition x is still understood). The hydrostatic and biaxial components of the strain along line scans in the z direction are plotted in Figs. 2 and 3 (cf. with Refs. 13 and 14).

In conclusion, the confinement potentials for the electron, the heavy, and the light holes in a QD are given by the differences between the energy bands of the GaAs and those of the $\text{In}_x\text{Ga}_{1-x}\text{As}$:

$$V^e(\rho, z) = E_c[x, z, S(\rho)] - E_c[0, z, S(\rho)], \quad (\text{A11})$$

$$V^{hh}(\rho, z) = E_v^{hh}[0, z, S(\rho)] - E_v^{hh}[x, z, S(\rho)], \quad (\text{A12})$$

$$V^{lh}(\rho, z) = E_v^{lh}[0, z, S(\rho)] - E_v^{lh}[x, z, S(\rho)], \quad (\text{A13})$$

where the dependence on the indium composition has been explicitly written.

Until now the indium composition x has been considered constant inside and zero outside the QD. In fact, when the

$\text{In}_x\text{Ga}_{1-x}\text{As}$ structure is grown, a considerable amount of indium atoms in a lower layer segregate to the upper one. This migration changes the profile of the indium composition, which, in the case of a QW, is usually approximated by the exponential shape²⁴

$$x(z) = \begin{cases} 0 & \text{if } z \leq 0 \\ x_0[1 - \exp(-z/\Lambda)] & \text{if } 0 < z \leq d \\ x_0[1 - \exp(-d/\Lambda)]\exp\left(-\frac{z-d}{\Lambda}\right) & \text{if } z > d, \end{cases} \quad (\text{A14})$$

where x_0 is the nominal indium composition, d is the QW thickness, and Λ is the segregation length. Thus we make the hypothesis that the segregation in a QD structure can be described in the same way. The function x is now given by

$$x[z, S(\rho)] = \begin{cases} 0 & \text{if } z \leq 0 \\ x_0[1 - \exp(-z/\Lambda)] & \text{if } 0 < z \leq S(\rho) \\ x_0\{1 - \exp[-S(\rho)/\Lambda]\}\exp\left(-\frac{z-S(\rho)}{\Lambda}\right) & \text{if } z > S(\rho), \end{cases} \quad (\text{A15})$$

where the QW thickness d has been replaced by the height profile of the QD, $S(\rho)$. If we insert this expression into Eqs. (A11), (A12), and (A13), we obtain, finally, Eqs. (21), (22), and (23).

APPENDIX B: GFDND PARAMETERS

The accuracy of the GFDND method can be improved by the choice of an appropriate transformation of variables that maps the infinite interval onto a finite one. We choose a transformation that has been proven to work very well.^{3,34} It maps the intervals $[0, +\infty)$ and $(-\infty, +\infty)$ onto $[0, 1)$ and $(0, 1)$, respectively, and it is given by

$$\bar{\rho} = 1 - e^{-\lambda_\rho \rho} \quad (\text{B1})$$

$$\bar{z} = \begin{cases} 1 - \frac{e^{-\lambda_z z}}{2} & z \geq 0 \\ \frac{e^{\lambda_z z}}{2} & z < 0, \end{cases} \quad (\text{B2})$$

where ρ and z are the original variables, and $\bar{\rho}$ and \bar{z} are the new ones.

The parameters λ_ρ and λ_z can be varied to optimize the accuracy of the numerical solution. If these parameters are too large, there is a loss of accuracy in the interpolation of the tails of the wave functions. On the other hand, if they are too small, there are too few grid points near the origin, where the wave functions and the potential change rapidly. Therefore, λ_ρ and λ_z should be chosen in order to have the grid points distributed on the whole interval where the wave functions are significantly different from zero. In practice, this condition can be satisfied by observing the plots obtained for the wave functions. In any case, the numerical results are very stable for quite a large range of values (see, Refs. 3 and 34). The number of grid points is equal to 100 for both variables, ρ and z , and the time step ε is equal to 0.1 (we have checked that smaller values do not significantly change the results).

Finally, we point out that to solve the eigenvalue problem we use the ARPACK package,³⁵ based on a restarted Lanczos/Arnoldi method. The code runs on a PC in a few minutes.

¹D. M. Ceperley, Rev. Mod. Phys. **67**, 279 (1995).

²J. W. Negele and H. Orland, *Quantum Many-Particle Systems* (Addison-Wesley, New York, 1988), p. 132.

³S. Taddei, J. Comput. Phys. **134**, 62 (1997).

⁴M. Rosa-Clot and S. Taddei, Phys. Rev. C **50**, 627 (1994).

⁵M. Rosa-Clot and S. Taddei, Phys. Lett. A **197**, 1 (1995).

⁶V. R. Manfredi, M. Rosa-Clot, L. Salasnich, and S. Taddei, Int. J. Mod. Phys. E **5**, 519 (1996).

⁷M. Colocci, A. Vinattieri, L. Lippi, F. Bogani, M. Rosa-Clot, S. Taddei, A. Bosacchi, S. Franchi, and P. Frigeri, Appl. Phys. Lett. **74**, 564 (1999).

⁸H. Jiang and J. Singh, Phys. Rev. B **56**, 4696 (1997).

- ⁹C. Pryor, Phys. Rev. B **57**, 7190 (1998).
- ¹⁰N. Makri and W. H. Miller, J. Chem. Phys. **90**, 904 (1989).
- ¹¹H. Kleinert, *Path-Integrals in Quantum Mechanics Statistics and Polymer Physics* (World Scientific, Singapore, 1990), p. 251.
- ¹²J. Y. Marzin and G. Bastard, Solid State Commun. **92**, 437 (1994).
- ¹³M. Grundmann, O. Stier, and D. Bimberg, Phys. Rev. B **52**, 11 969 (1995).
- ¹⁴M. A. Cusack, P. R. Briddon, and M. Jaros, Phys. Rev. B **54**, R2300 (1996).
- ¹⁵M. A. Cusack, P. R. Briddon, and M. Jaros, Phys. Rev. B **56**, 4047 (1997).
- ¹⁶D. M. Wood and A. Zunger, Phys. Rev. B **53**, 7949 (1996).
- ¹⁷A. Zunger, MRS Bull. **23**, 35 (1998).
- ¹⁸A. J. Williamson and A. Zunger, Phys. Rev. B **59**, 15 819 (1999).
- ¹⁹S. Taddei, M. Colocci, A. Vinattieri, F. Bogani, S. Franchi, P. Frigeri, L. Lazzarini, and G. Salviati (unpublished).
- ²⁰M. Berti, A. V. Drigo, A. Giuliani, M. Mazzer, A. Camporese, G. Rossetto, and G. Torzo, J. Appl. Phys. **80**, 1931 (1996).
- ²¹M. Colocci, F. Bogani, L. Carraresi, R. Mattolini, A. Bosacchi, S. Franchi, P. Frigeri, S. Taddei, and M. Rosa-Clot, Superlattices Microstruct. **22**, 81 (1997).
- ²²M. Colocci, F. Bogani, L. Carraresi, R. Mattolini, A. Bosacchi, S. Franchi, P. Frigeri, M. Rosa-Clot, and S. Taddei, Appl. Phys. Lett. **70**, 3140 (1997).
- ²³J. Y. Marzin, J. M. Gérard, A. Izraël, D. Barrier, and G. Bastard, Phys. Rev. Lett. **73**, 716 (1994).
- ²⁴K. Muraki, S. Fukatsu, Y. Shiraki, and R. Ito, Appl. Phys. Lett. **61**, 557 (1992).
- ²⁵L. Brusaferrri, S. Sanguinetti, E. Grilli, M. Guzzi, A. Bignazzi, F. Bogani, L. Carraresi, M. Colocci, A. Bosacchi, P. Frigeri, and S. Franchi, Appl. Phys. Lett. **69**, 3354 (1996).
- ²⁶F. Bogani, L. Carraresi, R. Mattolini, M. Colocci, A. Bosacchi, and S. Franchi, Solid-State Electron. **40**, 363 (1996).
- ²⁷A. Bosacchi and S. Franchi (private communication).
- ²⁸C. Ferrari, C. Bocchi, A. Bosacchi, and S. Franchi, Mater. Sci. Eng., B **B150**, 183 (1994).
- ²⁹A. Bosacchi, F. Colonna, S. Franchi, P. Pascarella, P. Allegri, and V. Avanzini, J. Cryst. Growth **150**, 185 (1995).
- ³⁰J. Brübach, A. Yu. Silov, J. E. M. Haverkort, W. van der Vleuten, and J. H. Wolter, Superlattices Microstruct. **21**, 527 (1997).
- ³¹P. D. Wang, N. N. Ledentsov, C. M. Sotomayor Torres, I. N. Yassievich, A. Pakhomov, A. Yu. Egovov, P. S. Kop'ev, and V. M. Ustinov, Phys. Rev. B **50**, 1604 (1994).
- ³²Chris G. Van de Walle, Phys. Rev. B **39**, 1871 (1989).
- ³³J. P. Reithmaier, R. Höger, H. Riechert, A. Heberle, G. Abstreiter, and G. Weimann, Appl. Phys. Lett. **56**, 536 (1990).
- ³⁴N. W. Schellingherhout, L. P. Kok, and G. D. Bosveld, Phys. Rev. A **40**, 5568 (1989).
- ³⁵R. B. Lehoucq, Argonne National Laboratory Report No. MCS-P591-0496, 1996 (unpublished).